AGU PUBLICATIONS

JGR

Journal of Geophysical Research: Atmospheres

RESEARCH ARTICLE

10.1002/2014JD022015

Special Section:
Fast Physics in Climate Models: Parameterization, Evaluation and Observation

Key Points:
- Sensitivity to the critical Richardson number is investigated with a GCM model
- Planetary boundary height increases with the critical Richard number
- Critical Richard number affects large scale and convective rainfall differently

Correspondence to:
Z. Gao
zgao@mail.iap.ac.cn

Citation:
Zhang, N., Z. Gao, Y. Liu, and D. Li (2015), Sensitivity of a global climate model to the critical Richardson number in the boundary layer parameterization, *J. Geophys. Res. Atmos.*, *120*, doi:10.1002/2014JD022015.

Received 23 MAY 2014
Accepted 24 MAR 2015
Accepted article online 26 MAR 2015

Sensitivity of a global climate model to the critical Richardson number in the boundary layer parameterization

Ning Zhang[1,2], Zhiqiu Gao[3], Yangang Liu[4], and Dan Li[5]

[1]Institute for Climate and Global Change Research and School of Atmospheric Sciences, Nanjing University, Nanjing, China, [2]Jiangsu Collaborative Innovation Center for Climate Change, Nanjing, China, [3]Laboratory of Atmospheric Physics and Chemistry, Institute of Atmospheric Physics, Beijing, China, [4]Biological, Environmental and Climate Sciences Department, Brookhaven National Laboratory, Upton, New York, USA, [5]Program of Atmospheric and Oceanic Sciences, Princeton University, Princeton, New Jersey, USA

Abstract The critical bulk Richardson number (Ri_{cr}) is an important parameter in planetary boundary layer (PBL) parameterization schemes used in many climate models. This paper examines the sensitivity of a global climate model, the Beijing Climate Center atmospheric general circulation model, to Ri_{cr}. The results show that the simulated global average of PBL height increases nearly linearly with Ri_{cr}, with a change of about 114 m for a change of 0.5 in Ri_{cr}. The surface sensible (latent) heat flux decreases (increases) as Ri_{cr} increases. The influence of Ri_{cr} on surface air temperature and specific humidity is not significant. The increasing Ri_{cr} may affect the location of the Westerly Belt in the Southern Hemisphere. Further diagnosis reveals that changes in Ri_{cr} affect stratiform and convective precipitations differently. Increasing Ri_{cr} leads to an increase in the stratiform precipitation but a decrease in the convective precipitation. Significant changes of convective precipitation occur over the Intertropical Convergence Zone, while changes of stratiform precipitation mostly appear over arid land such as North Africa and Middle East.

1. Introduction

The planetary boundary layer (PBL) is the part of the atmosphere where interactions between the atmosphere and the Earth's surface occur [*Stull*, 1988; *Liu et al.*, 2013]. Atmospheric flow in the PBL is characterized by strong turbulence that enhances transport and mixing of momentum, heat, moisture, and other quantities; hence, it is important to resolve or parameterize turbulence in atmospheric models. In most weather and climate models whose horizontal resolutions range from a few kilometers to a few hundreds of kilometers, turbulence cannot be resolved but is parameterized through so-called "PBL schemes." These PBL schemes can be broadly classified into two categories: *local* and *nonlocal*. A commonly used local scheme is the "*K*-theory" approach [*Louis,* 1979], in which turbulent fluxes (e.g., of momentum, heat, water vapor, and other passive scalars) are linked to the local mean gradients (e.g., of wind, potential temperature, specific humidity, and other variables) through an "eddy viscosity" or an "eddy diffusivity." The local scheme often fails when nonlocal transport is important (e.g., under strongly unstable or convective conditions) [*Stull*, 1988]. As such, nonlocal schemes have been developed to consider the nonlocal transport [*Troen and Mahrt*, 1986; *Louis*, 1979]. *Holtslag and Boville* [1993] compared local and nonlocal schemes in a global climate model (GCM), the National Center for Atmospheric Research Community Climate Model Version 2, and showed that the nonlocal scheme performed better under dry convective conditions.

The PBL height is an important parameter in most nonlocal schemes and is usually inferred from the *bulk* Richardson number [*Troen and Mahrt*, 1986; *Holtslag and Boville*, 1993], which is defined as the Richardson number for a layer from the surface to any height (z) above the surface. A key parameter to infer the PBL height from the bulk Richardson number is the *critical bulk* Richardson number (Ri_{cr}), which is the bulk Richardson number for the whole PBL [*Holtslag and Boville*, 1993; *Shin and Ha*, 2007; *Basu et al.*, 2014]. In the literature, many values have been used for this critical bulk Richardson number. For example, $Ri_{cr} = 0.5$ is typically used in GCMs with relatively coarse vertical resolutions [*Holtslag and Boville*, 1993; *Shin and Ha*, 2007]. A value of 0.3 is used in models with higher vertical resolutions, for instance, in the Community

Atmospheric Model version 3 (CAM3) [*Kiehl et al.*, 1998] and the Beijing Climate Center atmospheric general circulation model (BCC_AGCM) [*Wu et al.*, 2010]. $Ri_{cr} = 0.25$ is used in the Yonsei University planetary boundary layer scheme in the Weather Research and Forecasting model [*Noh et al.*, 2003]. Recent experimental studies also found that the critical bulk Richardson number has a strong dependence on the stability of the PBL [*Richardson et al.*, 2013; *Basu et al.*, 2014; *Zhang et al.*, 2014]. Here we note that other definitions of Richardson numbers are also often used in numerical models as well as observational/theoretical studies. For example, in the University of Washington moist turbulence scheme in CAM5 [*Bretherton and Park*, 2009; *Park and Bretherton*, 2009], which is a turbulent kinetic energy closure scheme, uses the moist *gradient* Richardson number to diagnose the vertical extent and stability characteristics of all turbulent layers in a model grid column. *Flux* Richardson number is often used in observational and theoretical studies [*Yamada*, 1975; *Grachev et al.*, 2013; *Katul et al.*, 2014]. It is particularly pointed out that the "*critical bulk* Richardson number" used in our study is different from the "*critical gradient* Richardson number" often associated with the Miles-Howard theory on the stability of laminar boundary layers whose value is about 0.25 [*Miles*, 1961].

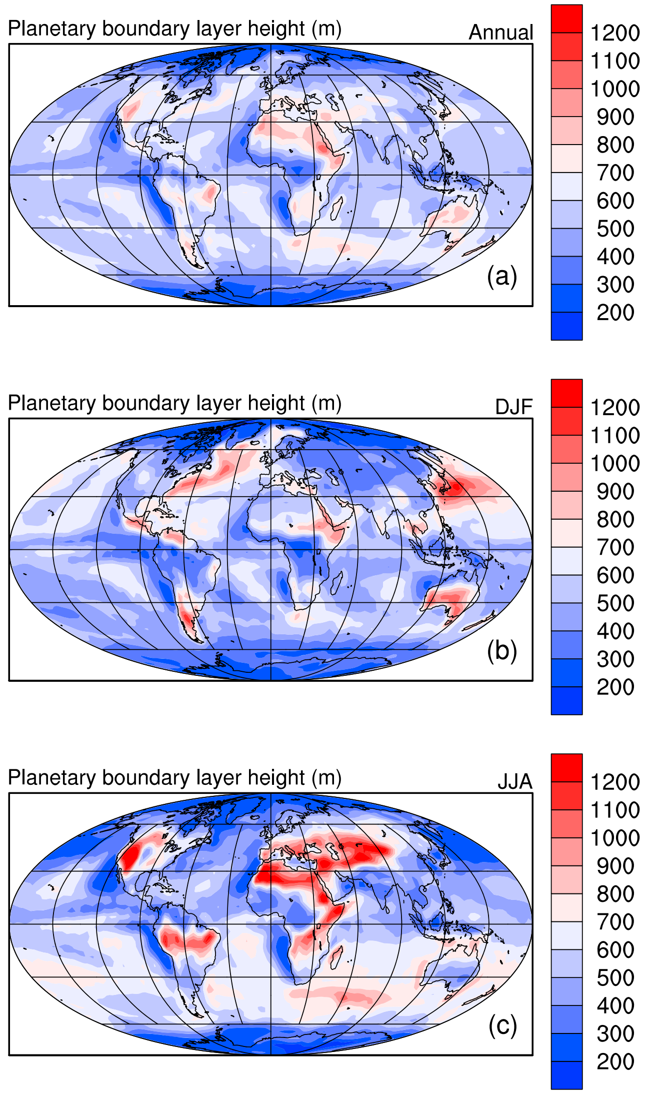

Figure 1. Simulated planetary boundary layer height in experiment CTL: (a) annual mean, (b) DJF mean, and (c) JJA mean.

The main objective of present work is to investigate the sensitivity of a GCM to the Ri_{cr} value in order to improve our PBL parameterizations in GCMs. To achieve this objective, this paper is organized as follows: a brief description of the BCC_AGCM model and the numerical experiments are described in section 2. The main results and discussions are presented in section 3 followed by a summary in section 4.

2. Model Description and Experiment Design

BCC_AGCM2.0.1 originates from the CAM3 but has been significantly modified as compared to CAM3. For example, the dynamic formulation in BCC_AGCM2.0.1 is different from the Eulerian spectral formulation in CAM3. BCC_AGCM2.0.1 uses a reference atmospheric temperature and a reference surface pressure, which induces changes in the governing equations and their solver [*Wu et al.*, 2008]. The revised Zhang and McFarlane's convection scheme [*Zhang and Mu*, 2005, hereafter RZM] is incorporated to replace the original scheme of *Zhang and McFarlane* [1995, hereafter ZM] in CAM3. The RZM scheme assumes that quasi equilibrium exists between convection and the large-scale environment in the free troposphere above the PBL. The cloud base mass flux is determined by the large-scale destabilization of the free troposphere due to changes in the free tropospheric temperature and moisture caused by large-scale

Table 1. The Simulated Globally Averaged PBL Height in Experiment CTL (Unit: m)

	Annual Mean			DJF Mean			JJA Mean		
	Global	Land	Ocean	Global	Land	Ocean	Global	Land	Ocean
Maximum	1113	1113	896	1279	1181	1279	1620	1619	1062
Minimum	194	194	208	184	186	184	146	146	191
Average	485	468	499	461	433	488	499	499	500

processes. The RZM scheme includes a relative humidity threshold (RH_c) as a convection trigger to suppress spurious convection when the PBL is dry. In addition, the bottom of an unstable lifted layer is allowed to occur above the PBL in the RZM scheme, while this level is limited to be below the top of the PBL in the RZM scheme. *Wu et al.* [2010] evaluated the model performance against the ERA-40 reanalysis and other observational data and found that BCC_AGCM2.0.1 well reproduces the present-day climate in terms of energy budgets, precipitation, sea level pressure, air temperature, geopotential height, atmospheric circulation, and their seasonal variations. Compared to the original CAM3, the new dynamical core and updated physical parameterizations in BCC_AGCM2.0.1 lead to an overall improvement in the simulation [*Wu et al.*, 2010].

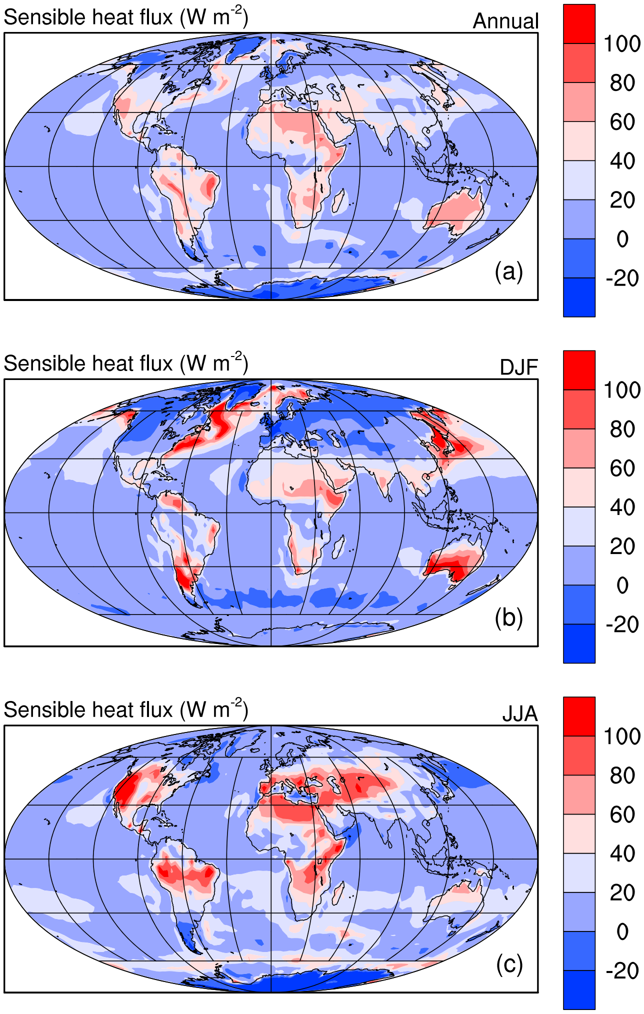

Figure 2. Same as Figure 1 but for sensible heat flux.

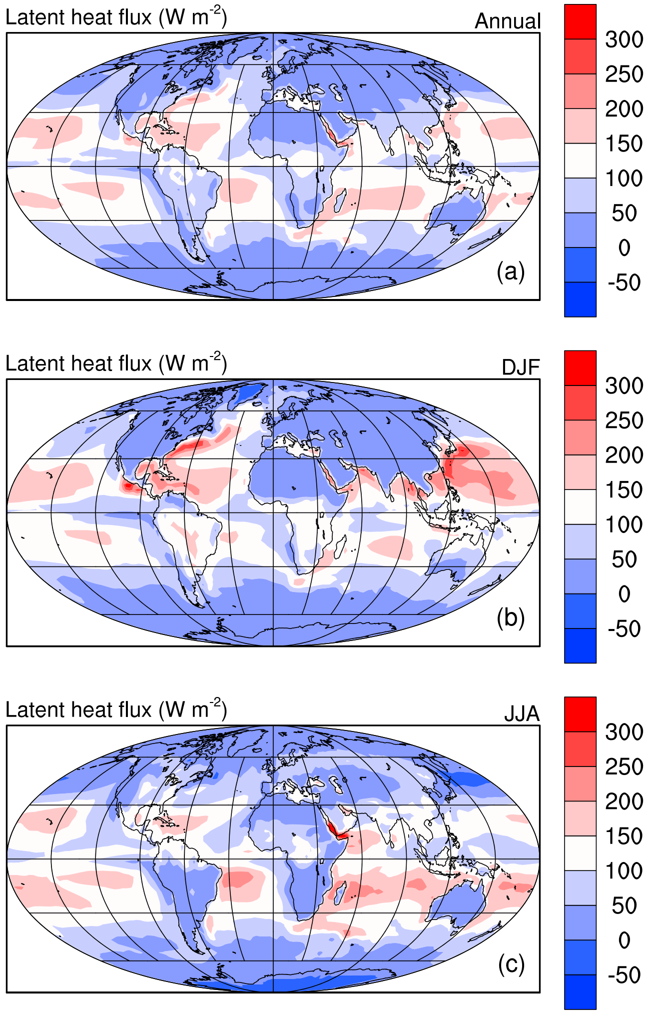

Figure 3. Same as Figure 1 but for latent heat flux.

In BCC_AGCM2.0.1, the free atmospheric turbulent diffusivities are typically taken as functions of length scales and local vertical gradients of wind and scalar variables, as in CAM3, and a nonlocal scheme is employed to parameterize turbulent flux in the PBL. In essence, the vertical flux of a constituent C (e.g., potential temperature, water vapor, or other passive scalars), $\overline{w'C'}$, is described by

$$\overline{w'C'} = -K_c\left(\frac{\partial \overline{C}}{\partial z} - \gamma_c\right), \tag{1}$$

where w is the vertical velocity and K_c is the eddy diffusivity of the constituent C; γ_c denotes the nonlocal transport term of C. The overbar denotes the Reynolds averaging, and the prime denotes turbulent fluctuations from the Reynolds average. The eddy diffusivity K_c is calculated through

$$K_c = \kappa w_t z\left(1 - \frac{z}{h}\right)^2, \tag{2}$$

where κ is the von Karman constant, w_t is a velocity scale as explained later, z is the height above the ground, and h is the PBL height. The nonlocal term is given by

$$\gamma_c = a\frac{w_*\overline{w'C'}_s}{w_m^2 h}, \tag{3}$$

where a is a constant, $w'C'_s$ is the surface flux, w_m is another turbulent velocity scale that is different from w_t, and w_* is the convective velocity scale ($w_* = \left[\frac{gh}{\overline{\theta}_v}\left(\overline{w'\theta'_v}\right)_s\right]^{1/3}$, where g is the gravitational constant, θ is the

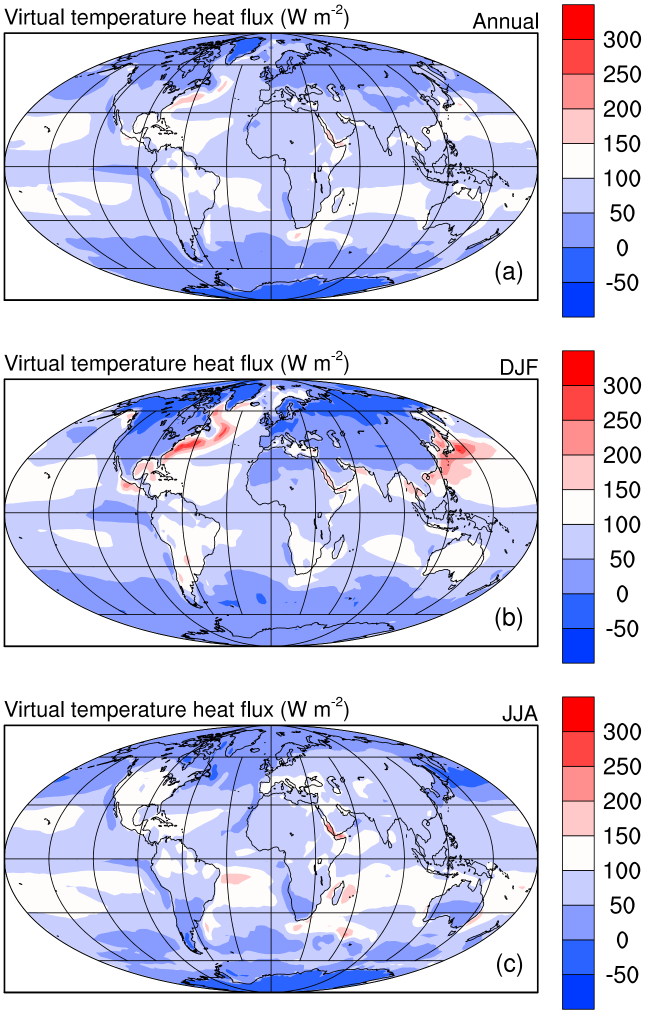

Figure 4. Same as Figure 1 but for virtual temperature heat flux.

potential temperature, and θ_v is the virtual potential temperature). Details on w_t and w_m can be found in *Troen and Mahrt* [1986]. Briefly, under unstable conditions, w_t and w_m are proportional to the convective velocity scale w_*. Under neutral and stable conditions, w_t and w_m are proportional to the surface friction velocity $u_* = \left[\overline{u'w'}^2 + \overline{v'w'}^2\right]^{1/4}$.

The PBL height h, used in equations (2) and (3), is given by *Vogelezang and Holtslag* [1996]:

$$h = z_s + \frac{Ri_{cr}\left[(u(h) - u_{SL})^2 + (v(h) - v_{SL})^2 + Bu_*^2\right]}{(g/\theta_{vSL})(\theta_v(h) - \theta_{vSL})}, \tag{4}$$

where z_s is the height of the atmospheric surface layer. The quantities u_{SL}, v_{SL}, and θ_{vSL} represent the horizontal wind components and virtual potential temperature at z_s, respectively. The quantities $u(h)$, $v(h)$, and $\theta_v(h)$ are the horizontal wind components and the virtual potential temperature at h, respectively. In practice, these quantities over the low model levels are used to iteratively determine h. The parameter B has been experimentally determined to be 100 [*Vogelezang and Holtslag*, 1996]. In a simplified form, equation (4) can be written as

$$h = z_s + \alpha Ri_{cr}, \tag{5}$$

where α is determined by surface friction velocity, wind speed, and potential temperatures at h. It is clear from the equations (1) to (5) that a change in Ri_{cr} will affect the PBL height h (equation (5)), which further leads to changes in the turbulent diffusivity (equation (2)) and turbulent fluxes (equation (1)).

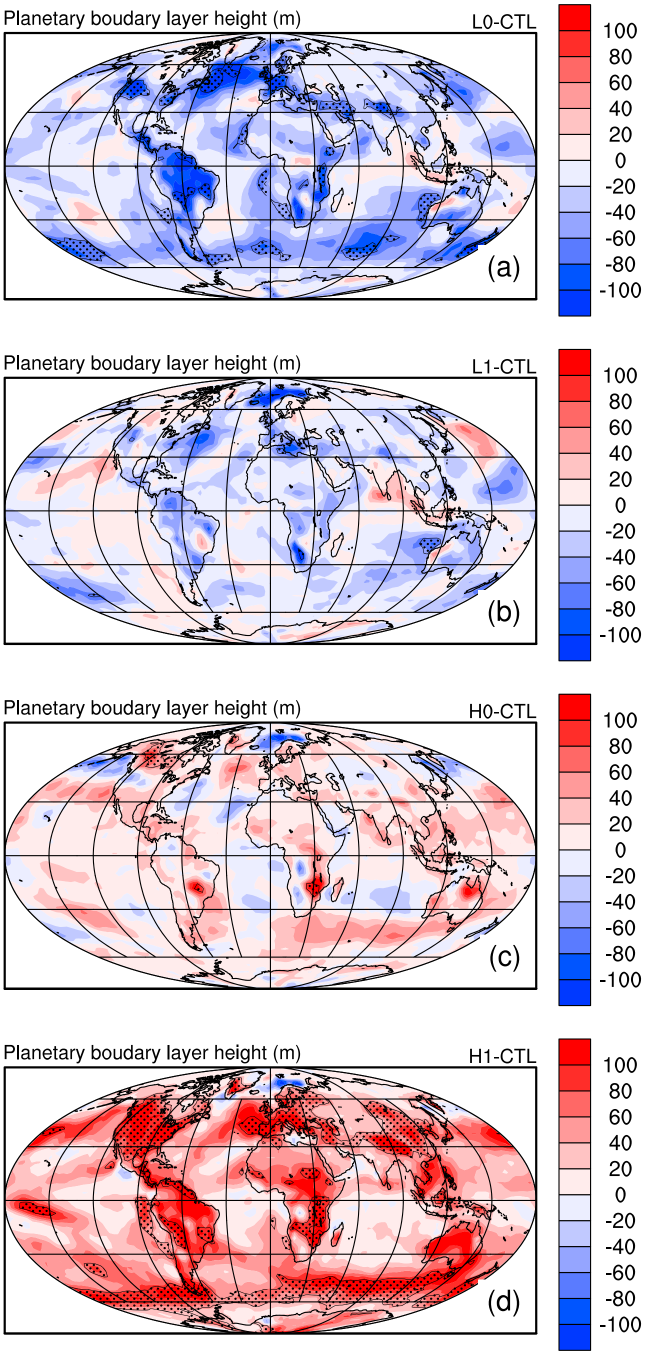

Figure 5. Annual mean differences of planetary boundary layer height between different experiments: (a) L0-CTL, (b) L1-CTL, (c) H0-CTL, and (d) H1-CTL (the dot-shadowed areas are where the statistical significance is less than 0.05 with the Student's *t* test).

To examine the impact of Ri_{cr} on model output, a suit of 50 year simulations with five values of Ri_{cr} (0.19, 0.25, 0.30, 0.35, and 0.50) are carried out, denoted as L0, L1, (control) CTL, H0, and H1, respectively. These values are chosen to span the range of Ri_{cr} values commonly used in climate models, as reviewed in the Introduction. All simulations started from 1 September 1950 with the atmospheric conditions, soil moistures, and snow cover/depth initialized from a previous model simulation and the sea surface temperature (SST) data taken from the Halley Center SST observational data. The model was run with horizontal resolution of T42 (approximately 2.8° latitude × 2.8° longitude grid), and 26 vertical levels with a rigid lid at 2.914 hPa, and an

Table 2. The Simulated Annual Mean Difference and Relative Change of Planetary Boundary Layer Height (PBLH), Sensible Heat Flux (SHFLX), Latent Heat Flux (LHFLX), and Total Precipitation

		Difference			Relative Change (%)		
		Global	Land	Ocean	Global	Land	Ocean
PBLH (m)	L0:$Ri_{cr} = 0.19$	−25.7	−26.4	−25.0	−2.31	−2.41	−2.80
	L1:$Ri_{cr} = 0.25$	−11.7	−11.8	−11.5	−1.15	−1.06	−1.28
	H0:$Ri_{cr} = 0.35$	11.0	12.1	10.1	0.99	1.09	0.91
	H1:$Ri_{cr} = 0.50$	44.8	48.6	41.4	4.02	4.37	4.62
SHFLX ($W m^{-2}$)	L0:$Ri_{cr} = 0.19$	0.44	0.28	0.59	2.11	1.32	2.82
	L1:$Ri_{cr} = 0.25$	0.20	0.10	0.28	0.94	0.49	1.35
	H0:$Ri_{cr} = 0.35$	−0.19	−0.17	−0.21	−0.92	−0.83	−1.01
	H1:$Ri_{cr} = 0.50$	−0.84	−0.67	−0.99	−3.99	−3.20	−4.70
LHFLX ($W m^{-2}$)	L0:$Ri_{cr} = 0.19$	−0.24	−0.14	−0.34	−0.37	−0.21	−0.52
	L1:$Ri_{cr} = 0.25$	−0.07	0.00	−0.13	−0.11	0.00	−0.20
	H0:$Ri_{cr} = 0.35$	0.12	0.17	0.08	0.19	0.25	0.12
	H1:$Ri_{cr} = 0.50$	0.46	0.38	0.53	0.70	0.58	0.80
Total precipitation ($mm yr^{-1}$)	L0:$Ri_{cr} = 0.19$	−4.20	−3.80	−4.56	−0.63	−0.57	−0.68
	L1:$Ri_{cr} = 0.25$	−1.38	0.61	−3.18	−0.21	0.09	−0.48
	H0:$Ri_{cr} = 0.35$	2.39	3.92	1.01	0.36	0.59	0.15
	H1:$Ri_{cr} = 0.50$	6.70	7.76	5.74	1.00	1.16	0.86

output frequency of 6 h. The first 20 years were treated as the spin-up period, and the analyses only focused on the last 30 years (i.e., 1971 to 2000).

3. Results and Discussions

3.1. Sensitivities of Simulated PBL Height and Surface Fluxes to Ri_{cr}

The global distributions of annual mean, DJF (December, January, and February) mean, and JJA (June, July, and August) mean PBL height simulated in the CTL experiment (i.e., $Ri_{cr} = 0.3$) are shown in Figure 1. The PBL height is averaged over the entire diurnal circle. As can be seen, the PBL height is more variable over land than over ocean. Deeper boundary layers occur in North Africa, the west part of North America, and west Australia. This is because the land cover types in these areas are desert or mountains with larger surface heating rate. The boundary layer is also deeper in regions with strong winds, such as the Southern Hemisphere storm track and the trade wind region. PBL depths are lower at higher latitudes, resulting from a colder surface and thus stronger static stability.

The annual mean global average of PBL height is 485 m, ranging from 194 m to 1113 m (Table 1), and both the maximum and minimum of annual mean PBL height occur over land. Over ocean, the maximum and minimum PBL heights are 896 m and 208 m, respectively, with an annual mean of 499 m (as compared to 468 m over land). In DJF, deeper PBLs appear over ocean, especially over the Gulf Stream and Kuroshio in the Northern Hemisphere because there are large temperature differences between the cold air and the warm sea surface. In the Southern Hemisphere, deeper PBLs occur over west Australia and the southern part of South America. In JJA, the PBL heights appear to be higher over land where there are larger surface heating rates. The average PBL heights over west North America, the north-middle part of South America, North Africa, the south Europe, and the middle Asia are all above 1000 m.

Figures 2 and 3 show the annual mean, DJF mean, and JJA mean sensible heat flux and latent heat flux, respectively. There is a good correspondence between the patterns of PBL height and sensible heat flux, with correlation coefficients of 0.64, 0.63, and 0.71 for annual mean, DJF mean, and JJA mean, respectively. This is expected because they are coupled in the model via equations (1) to (4). A higher sensible heat flux leads to stronger instability and stronger turbulent mixing and hence higher PBL height. This is particularly the case over land. The correlation coefficient between annual mean PBL height and sensible heat flux over land is 0.71. In comparison, the PBL height is less correlated with latent heat flux, with an annual mean correlation coefficient of 0.57. It is interesting to note that the PBL height exhibits better correlations with the surface virtual temperature flux (Figure 4), with correlation coefficients of 0.74, 0.79, and 0.72 for annual mean, DJF mean, and JJA mean. The correlation coefficients between annual mean PBL height and surface virtual temperature flux over land and over ocean are same (=0.78).

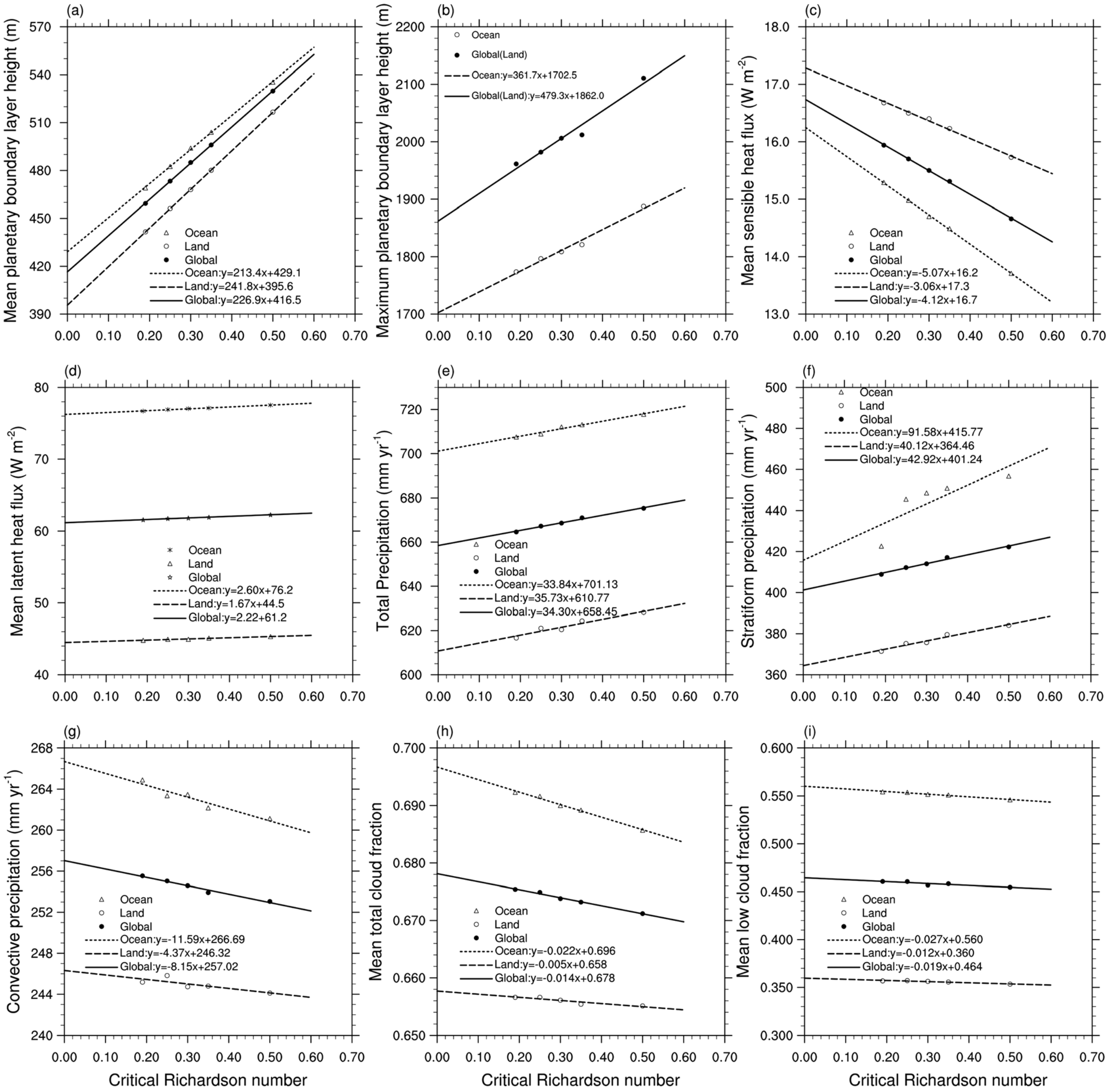

Figure 6. Simulated (a) mean planetary boundary layer height, (b) maximum planetary boundary layer height, (c) mean sensible heat flux, (d) mean latent heat flux, (e) total precipitation, (f) stratiform precipitation, (g) convective precipitation, (h) mean total cloud fraction, and (i) mean low cloud fraction in different cases as a function of Ri_{cr}.

Figure 5 shows the differences in the annual mean PBL height between the sensitivity experiments and the CTL experiment (results of L0, L1, H0, and H1 experiments minus CTL experiment results). The Student's *t* test is used to calculate the significance of PBL height change at each model grid cell, and the shadow areas are where the significance level is less than 0.05. It is clear that changes in the simulated PBL height are not spatially homogeneous. In the L1 and H0 experiments, changes in most model grids did not pass the significance test, while in the H1 experiment, significant changes appear over land in the Northern Hemisphere, including North America, Europe, East Asia, and the Tibetan Plateau. Changes over the Southern Hemisphere mainly occur over the ocean around 45–60°S. The averaged PBL height in this area decreases by 38.0 m in the L0 experiment and increases by 64.2 m in the H1 experiment.

The global-averaged differences in the PBL height between the L0, L1, H0, and H1 experiments and the CTL experiment are −25.7 m, −11.7 m, 11.0 m, and 44.8 m, respectively (Table 2). The differences over land are slightly larger than those over the ocean. The differences between the L0, L1, H0, and H1 experiments and

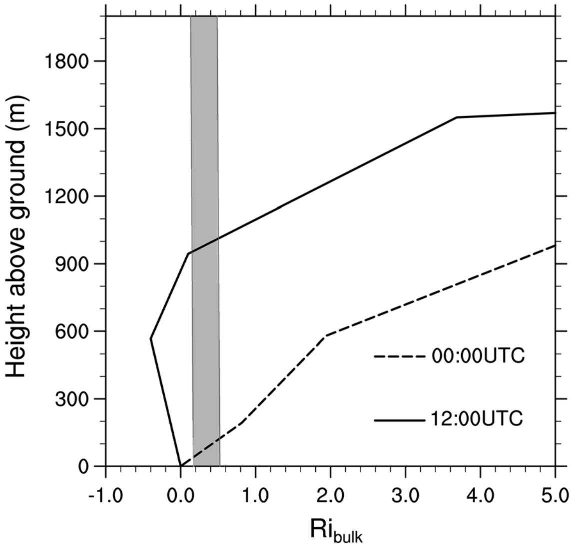

Figure 7. The vertical profile of the bulk Richardson number over west Sahara desert at 00:00 UTC (stable) and 12:00 UTC (unstable) on a typical day in July 2000.

the CTL experiment are −26.4 m, −11.8 m, 12.1 m, and 48.6 m over land, respectively, and are −25.0 m, −11.5 m, 10.1 m, and 41.4 m over ocean, respectively (see Table 2). Figure 6a further indicates that the PBL height increases as the Ri_{cr} increases and the relationship is nearly linear. The globally averaged annual mean PBL height increases by about 114 m per a change of 0.5 in Ri_{cr}, with a slightly higher rate of change over land (121 m) than over ocean (106 m).

The maximum PBL height also increases nearly linearly as Ri_{cr} increases, as can be seen from Figure 6b. The global maximum PBL height, which occurs over land in all experiments, increases by 240 m when Ri_{cr} increases by 0.5, and the maximum of PBL height over ocean increases by 181 m for an Ri_{cr} increase of 0.5. The minimum PBL height does not change with Ri_{cr} in all the experiments because it is set as the height of the lowest model level to maintain numerical stability and to prevent complete collapse of mixing under strongly stable conditions. The relative changes of global mean in different experiments are also calculated. The relative changes of PBL height between L0, L1, H0, and H1 experiments and the CTL experiment are −2.31%, −1.15%, 0.99%, and 4.02%. The relative changes over ocean are slightly larger than these over land area because of the lower marine PBL heights (Table 2).

The linear relationship between Ri_{cr} and the mean/maximum PBL height can be explained by the vertical distribution of the bulk Richardson number. Figure 7 shows the vertical profiles of the bulk Richardson number at 00:00 UTC and 12:00 UTC over the west Sahara desert on a clear-sky day in July 2000 (the local standard time is nearly same to the UTC time at this location). At 00:00 UTC, when a stable PBL occurs, the bulk Richardson number increases nearly linearly throughout the whole PBL. As a result, an increase in the value of Ri_{cr} leads to an increase in the PBL height nearly linearly under stable conditions. At 12:00 UTC, the bulk Richardson number is nearly zero in the PBL because the potential temperature gradient becomes very weak under the influence of convection. Just above the PBL, the bulk Richardson number usually increases rapidly across a very shallow layer because of a sharp increase in potential temperature. However, in our simulations, the vertical resolution of a GCM model is too coarse (26 vertical levels in total and only 5 to 6 levels under 2 km) to capture such a rapid change, and the PBL height is usually determined by a linear interpolation between two model levels, one with a bulk Richardson number smaller than Ri_{cr} and the other with a bulk Richardson number larger than Ri_{cr} (which occurs in the free atmosphere). Given that the bulk Richardson number increases nearly linearly in the free atmosphere under unstable conditions, the PBL height diagnosed through this interpolation also increases linearly as the value of Ri_{cr} increases. Consequently, the PBL height increases nearly linearly with Ri_{cr} under both stable and unstable conditions.

Figure 6c shows that the globally averaged annual mean sensible heat flux decreases with increasing Ri_{cr}. The globally averaged differences between L0, L1, H0, and H1 experiments and CTL experiment are 0.44, 0.20, −0.19, and −0.84 W m^{-2}, respectively (Table 2). As such, the global sensible heat flux decreases by about 2.06 W m^{-2} when Ri_{cr} increases by 0.5; the rate of change is smaller over land (−1.53 W m^{-2}) but larger over ocean (−2.535 W m^{-2}). The globally averaged relative changes of sensible heat flux are 2.11%, 0.94%, −0.92%, and −3.99% in L0, L1, H0, and H1 experiments, respectively (Table 2). The simulated sensible heat flux responds more significantly to the changes in Ri_{cr} over the high-middle-latitude ocean (30–70°S) in the Southern Hemisphere than over other areas, as can be seen from Figure 8. The globally averaged annual mean differences in sensible heat flux over this area between L0, L1, H0, and H1 experiments and CTL experiment are 0.76, 0.19, 0, −0.33, and −1.32 W m^{-2}, respectively.

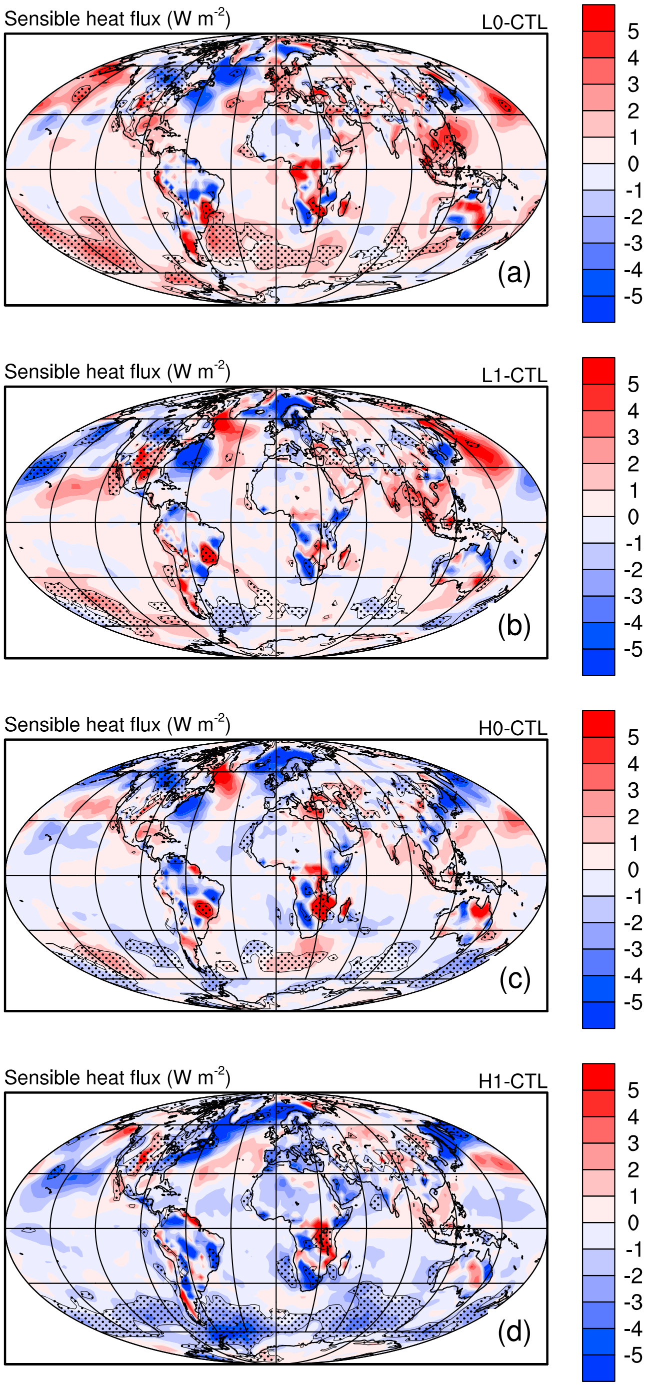

Figure 8. Same as Figure 4 but for sensible heat flux.

Unlike sensible heat flux, the globally averaged annual mean of latent heat flux increases with increasing Ri_{cr} (Figure 6d). When Ri_{cr} increases by 0.5, the annual mean latent heat flux over the globe, land, and ocean increases approximately by 1.10 W m^{-2}, 0.83 W m^{-2}, and 1.30 W m^{-2}, respectively. The globally averaged annual mean differences in latent heat flux between L0, L1, H0, and H1 experiments and CTL experiment are -0.24, -0.07, 0.12, and 0.46 W m^{-2}, respectively (Table 2). These differences are only half of those of sensible heat fluxes, and the relative changes of latent heat flux are also much less than those of sensible heat flux because of the much larger globally averaged annual mean of latent heat flux. However, although the global-averaged changes in latent heat flux are smaller than those in sensible heat flux, the

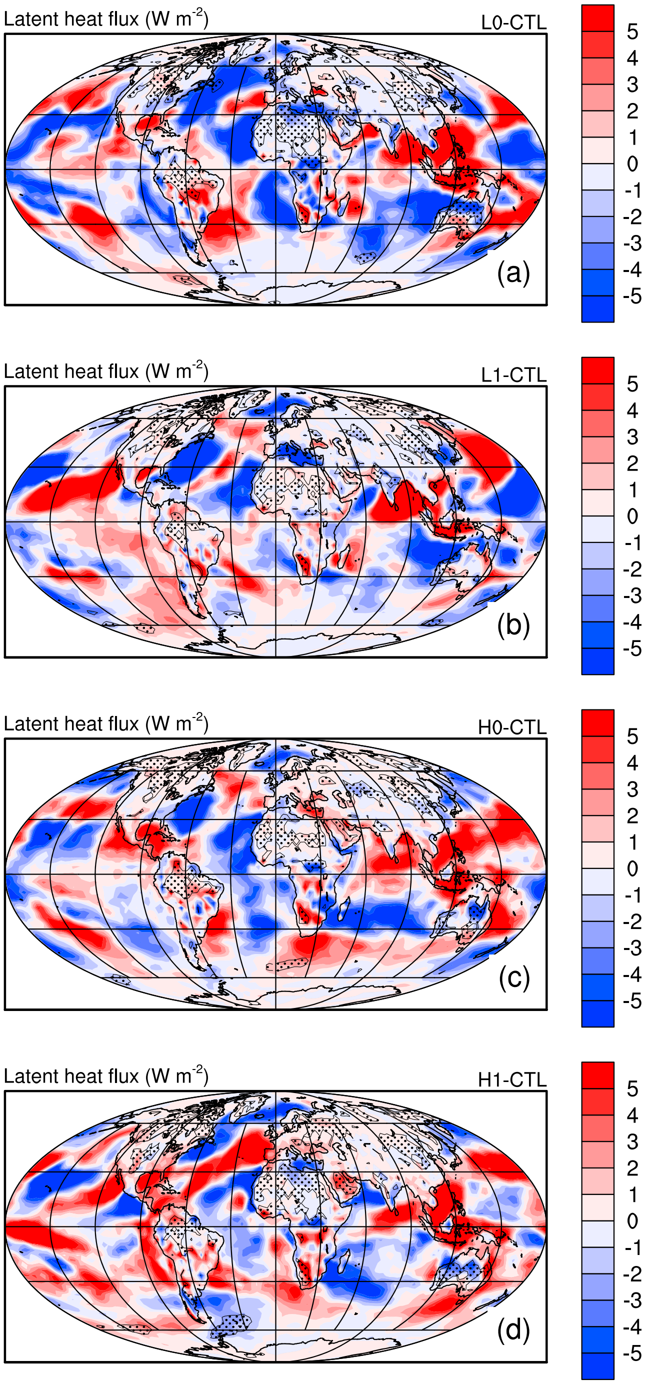

Figure 9. Same as Figure 4 but for latent heat flux.

spatial distribution is more heterogeneous. As can be seen from Figure 9, changes in latent heat flux mostly occur over the subtropical ocean. However, changes over land are more statistically significant, especially over arid areas such as the North Africa, Australia, Mongolian, and north China. Again, the Student's *t* test is used to calculate the significance of latent heat flux change at each model grid cell, and the shadow areas show where the significance level is less than 0.05. This is due to the significant changes in the stratiform precipitation as shall be discussed in section 3.3, which affects soil moisture and then latent heat flux in these areas.

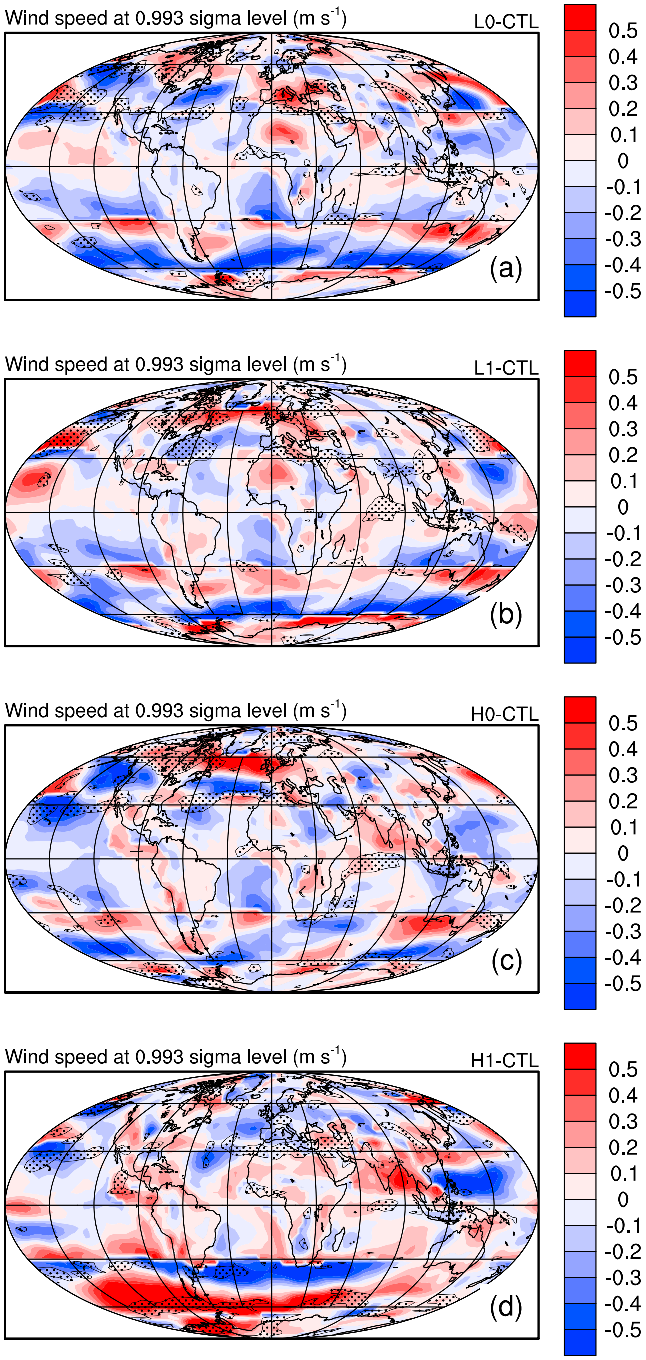

Figure 10. Same as Figure 4 but for wind speed at 0.993 sigma level.

3.2. Sensitivities of Wind, Temperature, and Humidity Fields to Ri_{cr}

Changes in the global mean wind speed are small in all sensitivity experiments (less than 0.05 m s^{-1} at all vertical levels), and relative changes are no larger than 0.5%. Significant changes occur over the Westerly Belt area in the Southern Hemisphere. The surface wind speed (at the level of 0.993 sigma in the model) increases over the high-latitude area (45–65°S) but decreases over the middle-latitude area (25–45°S) as Ri_{cr} increases, as shown in Figure 10. It is also noted that this phenomenon appears at all model levels below the 0.266 sigma level. Figure 11 further shows changes of the west-east component in the sensitivity experiments, and it is clear that increasing Ri_{cr} strengthens the west-east wind component over

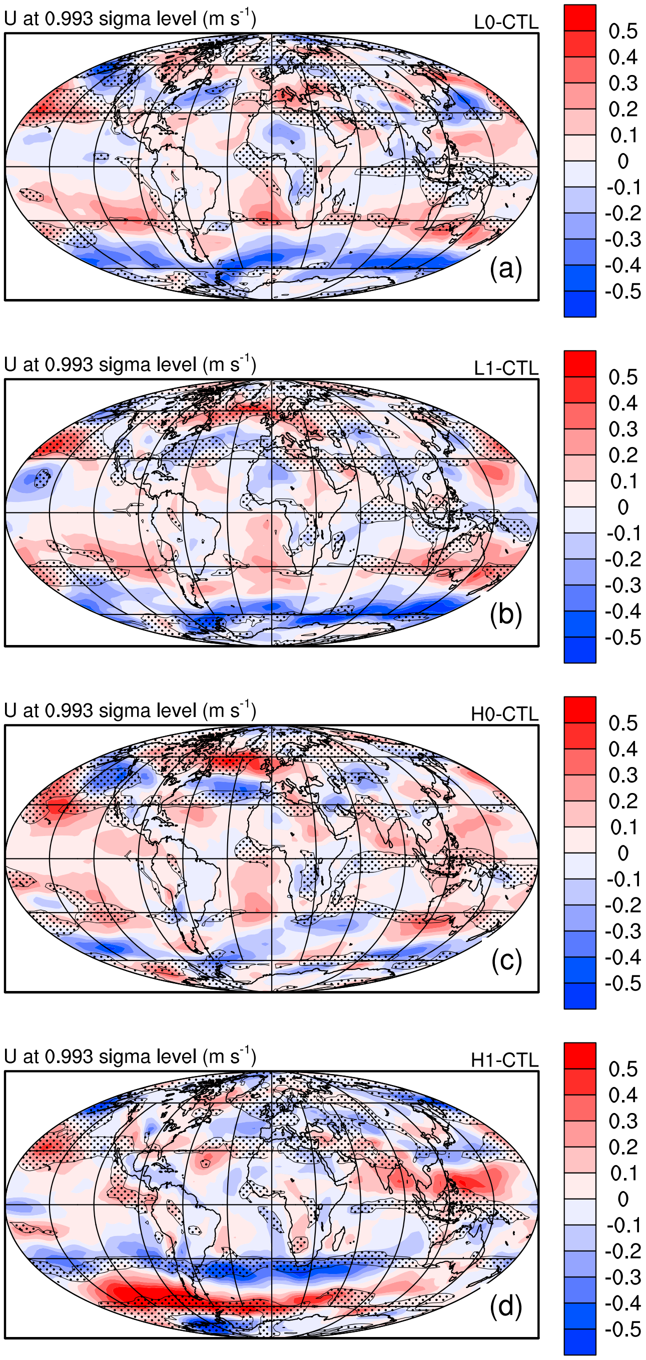

Figure 11. Same as Figure 4 but for the west-east wind component at 0.993 sigma level.

the area around 60°S and weakens the west-east wind component over the area around 30°S. This will be further discussed in section 3.4.

Changes in air temperature and specific humidity between the sensitivity experiments and the CTL experiment are insignificant at the significance level of 0.05 (not shown). The global-averaged changes in annual mean air temperature in all experiments are less than 0.2 K, and the relative changes are less than 0.5%. For specific humidity, the changes at all vertical levels are less than 0.001 g kg^{-1}, and the relative changes are less than 1.0%.

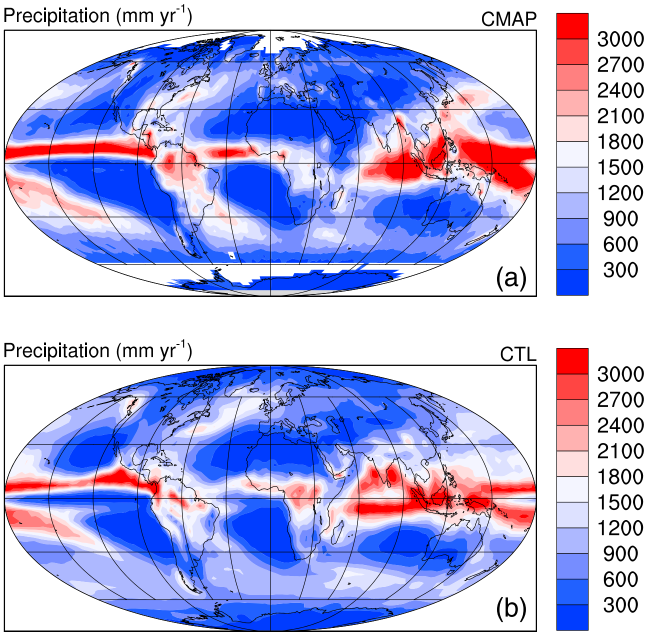

Figure 12. Comparison of (a) the Climate Prediction Center Merged Analysis of Precipitation (CMAP) data and (b) simulated global precipitation.

3.3. Sensitivities of Precipitation and Cloud to Ri_{cr}

Precipitation and cloud processes are known to be sensitive to PBL schemes [*Holtslag and Boville*, 1993; *Shin and Ha*, 2007; *Yao and Cheng*, 2012]. The simulated precipitation in the CTL experiment is first validated against the CMAP (Climate Prediction Center Merged Analysis of Precipitation) precipitation data as shown in Figure 12. It is evident that the model reproduces the global precipitation distribution fairly well, but the model underestimates the precipitation over the Intertropical Convergence Zone (ITCZ) and in Brazil and overestimates the precipitation over India and middle Africa. All numerical experiments underestimate the global mean precipitation with a bias close to $-80\,\text{mm yr}^{-1}$, and the model yields a better simulation over Brazil and India in the experiment H1, in which $Ri_{cr} = 0.50$. Our simulations show that global mean precipitation increases with increasing Ri_{cr}. Differences between the L0, L1, H0, and H1 experiments and the CTL experiment are -4.20, -1.38, 2.39, and $6.70\,\text{mm yr}^{-1}$, respectively. The differences over ocean are larger than over land (see Table 2).

The fact that the total precipitation increases with increasing Ri_{cr}, as shown in Figure 6e, is consistent with changes in surface latent heat flux, suggesting more effective exchanges of moisture between the land surface and the atmosphere occurring in experiments with higher Ri_{cr} values. In the model, the total precipitation is composed of stratiform precipitation and convective precipitation, which are treated differently. It is interesting to note that the effects of increasing Ri_{cr} on convective and stratiform precipitations are distinct (cf., Figures 13 and 14). Globally averaged stratiform precipitation increases, but convective precipitation decreases with increasing Ri_{cr} (as can be also seen from Figures 6f and 6g). The increasing rate of stratiform precipitation is stronger than the decreasing rate of convective precipitation, resulting in an increasing rate of total precipitation as Ri_{cr} increases. Furthermore, strong and significant changes in convective precipitation occur over the ITCZ in the sensitivity experiments (Figure 13). The absolute differences can be larger than $100\,\text{mm yr}^{-1}$ due to changes in the precipitation pattern. The changes in convective precipitation over North America, East Europe, Siberia, Australia, and the Westerly Belt also pass the significance test but are relatively weaker since the absolute differences in these areas are less than $20\,\text{mm yr}^{-1}$. The spatial distribution of changes in stratiform precipitation is more homogeneous in the sensitivity experiments (see Figure 14), and the most significant changes occur over land, especially over North Africa, Arabian Peninsula, Indian, and East Asia. The areas passing the significance test agree well with those of latent heat flux (see Figure 9). As mentioned earlier, this

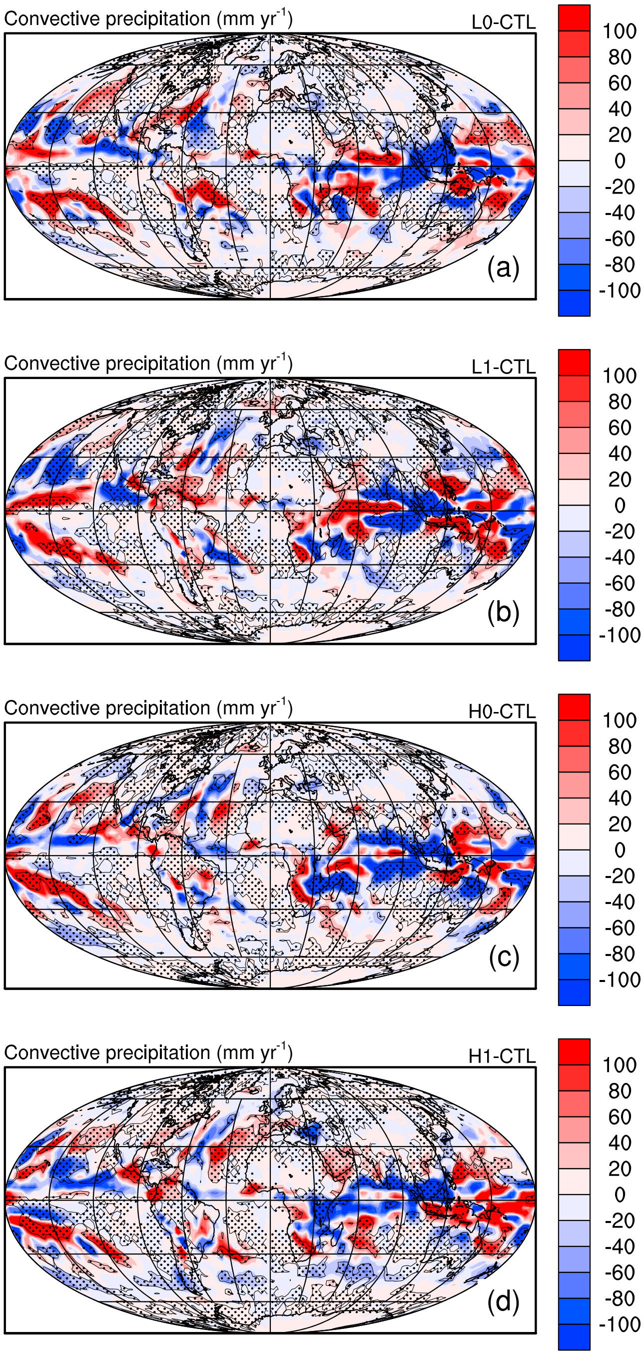

Figure 13. Same as Figure 4 but for the convective precipitation.

demonstrates that changes in stratiform precipitation in these relatively arid areas impact the soil moisture and then the exchange of water between the land surface and the atmosphere.

Changes in Ri_{cr} also affect cloud fraction but only marginally and insignificantly. The globally averaged differences in cloud fraction between L0, L1, H0, and H1 experiments and CTL experiment are less than 1%, and the local maximum changes are only 4%. The global mean cloud fraction decreases with increasing Ri_{cr}, and changes over ocean are larger than over land. When Ri_{cr} increases by 0.5, the cloud fractions over the globe, land, and ocean decrease approximately by 0.007, 0.005, and 0.011, respectively (Figure 6h). Changes in Ri_{cr} affect the low cloud more than the high cloud (as expected): when Ri_{cr}

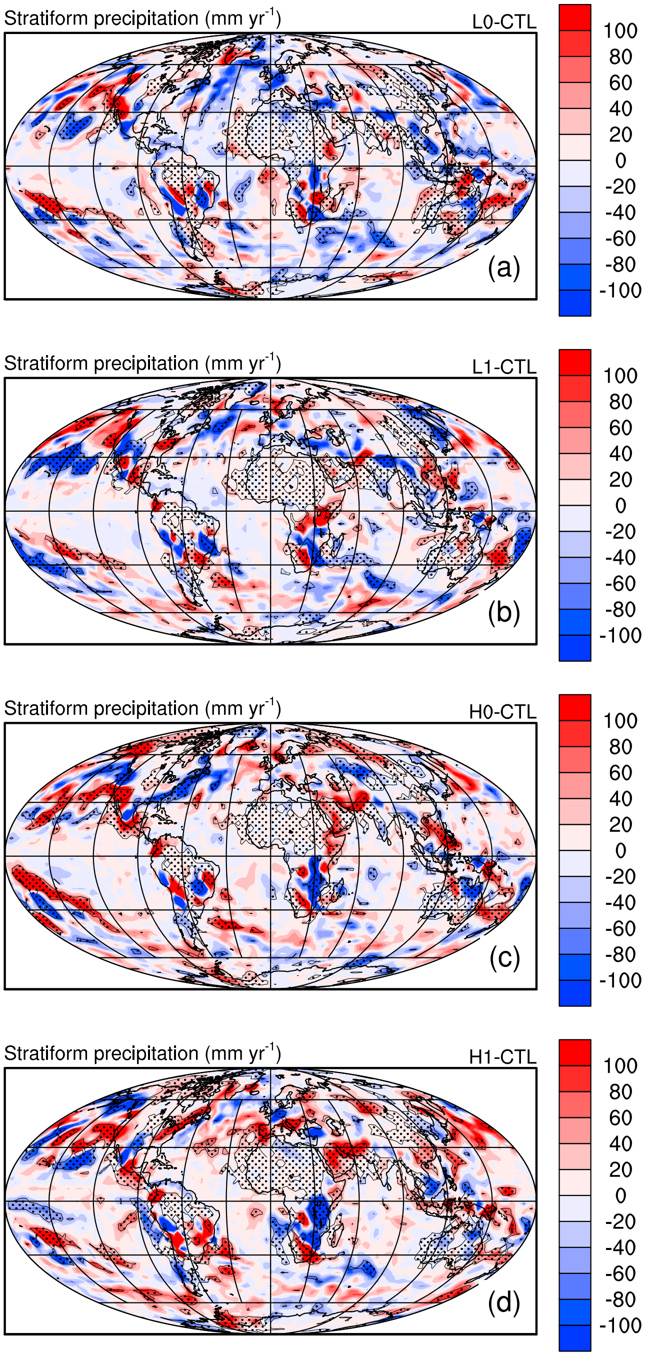

Figure 14. Same as Figure 4 but for the stratiform precipitation.

increases by 0.5, the low cloud fractions over the globe, land, and ocean decrease approximately by 0.009, 0.006, and 0.014, respectively (Figure 6i). The influence on the low cloud fraction is more significant over land, including North Africa, Middle East, South America, and Australia (Figure 15).

Figure 16 illustrates changes in the lifting condensation level (LCL) in different sensitivity experiments. As can be seen, most of the changes in the LCL occur over land, such as North Africa, America, Australia, and East Asia. Because LCL is determined by several meteorological variables such as air temperature and relative humidity, the response of the LCL to changing Ri_{cr} is more complicated. For example, the differences in the center of South America are always positive, while the differences in North Africa are negative in the

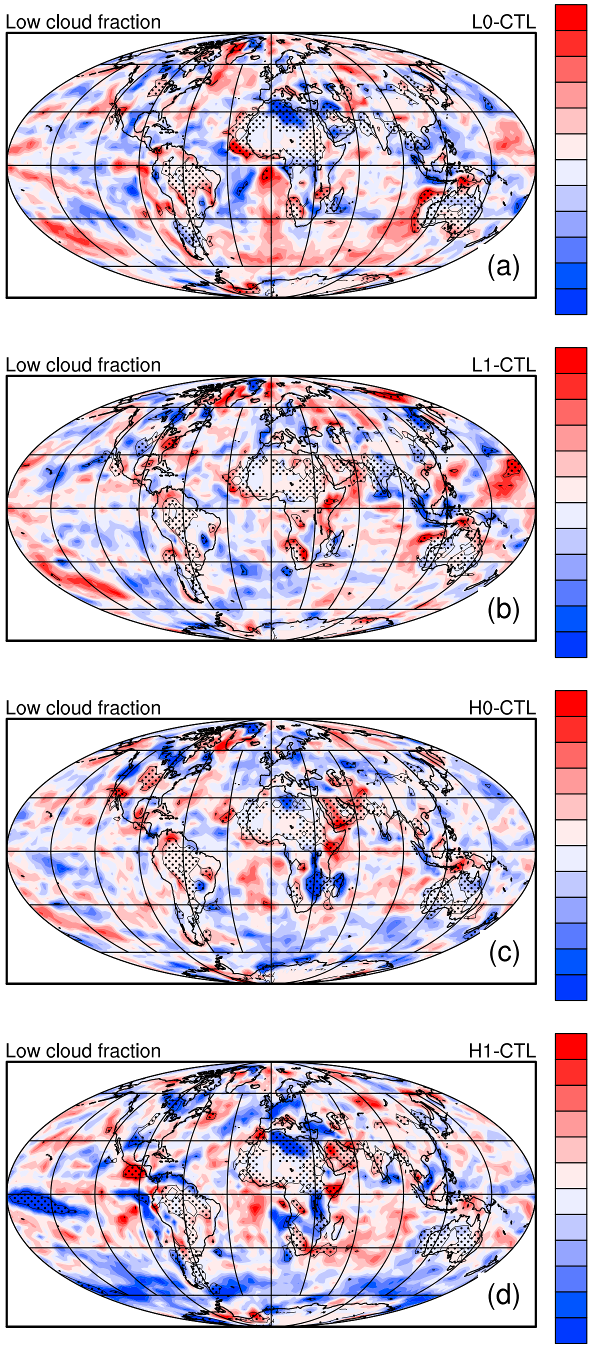

Figure 15. Same as Figure 4 but for low cloud fraction.

L0 and H1 experiments. The areas where the changes in LCL passing the statistical test are not consistent with the areas where the changes in convective precipitation passing the statistical test, which demonstrates the complicated nature of the precipitation processes [e.g., *Findell and Eltahir*, 2003].

3.4. Impacts on Regional Climate Simulations in the H1 Experiment

Although globally averaged influences on the PBL height, surface fluxes, and other meteorological fields seem relatively small, the spatial distributions of these impacts are inhomogeneous and thus are more significant over some areas. This section focuses on the impacts of changing Ri_{cr} in the Southern Hemisphere in the H1 experiments, because (i) the Ri_{cr} value (=0.5) in the H1 experiment is widely used in previous GCM simulations and (ii) the Westerly Belt in the Southern Hemisphere is a region most sensitive to the changes in Ri_{cr}.

In the H1 experiment, the PBL height increases over the whole middle-high-latitude ocean area in the Southern Hemisphere (30°S–65°S) compared to the CTL experiment. The averaged increase over model grid cells that pass the significance test in this area is 82.5 m, with the maximum increase of 221.7 m occurring near the coastal line of Australia and the minimum of 34.7 m occurring over the South Atlantic Ocean near the Drake Passage. This is because the H1 experiment simulates an increase in air temperature in this area and the maximum increase of 0.6 K occurs at the 0.787 sigma level (not passing the significance test). This makes the local PBL more stable and inhibits changes in the PBL height. At the same time, the increasing near-surface air temperature also causes decreasing surface sensible heat flux. In this area, the averaged change in sensible heat flux over grid cells passing the significant test is $-2.21\,\mathrm{W\,m^{-2}}$, and the minimum is $-7.18\,\mathrm{W\,m^{-2}}$, which also occurs at the Drake Passage. The simulated latent heat flux is not sensitive to the changes in Ri_{cr} in most part of this area (30°S–65°S), but it should be noted that a decrease in latent sensible heat flux also appears near the Drake Passage with an average decrease of $-0.97\,\mathrm{W\,m^{-2}}$. The H1 experiment also shows an increase of the west-east wind component around 60°S and a decrease around 30°S. The averaged increase around 60°S over the significant grid cells is $0.30\,\mathrm{m\,s^{-1}}$ at the 0.993 sigma level, and the maximum increase is $0.34\,\mathrm{m\,s^{-1}}$ at the 0.510 sigma level. The averaged decrease around 30°S

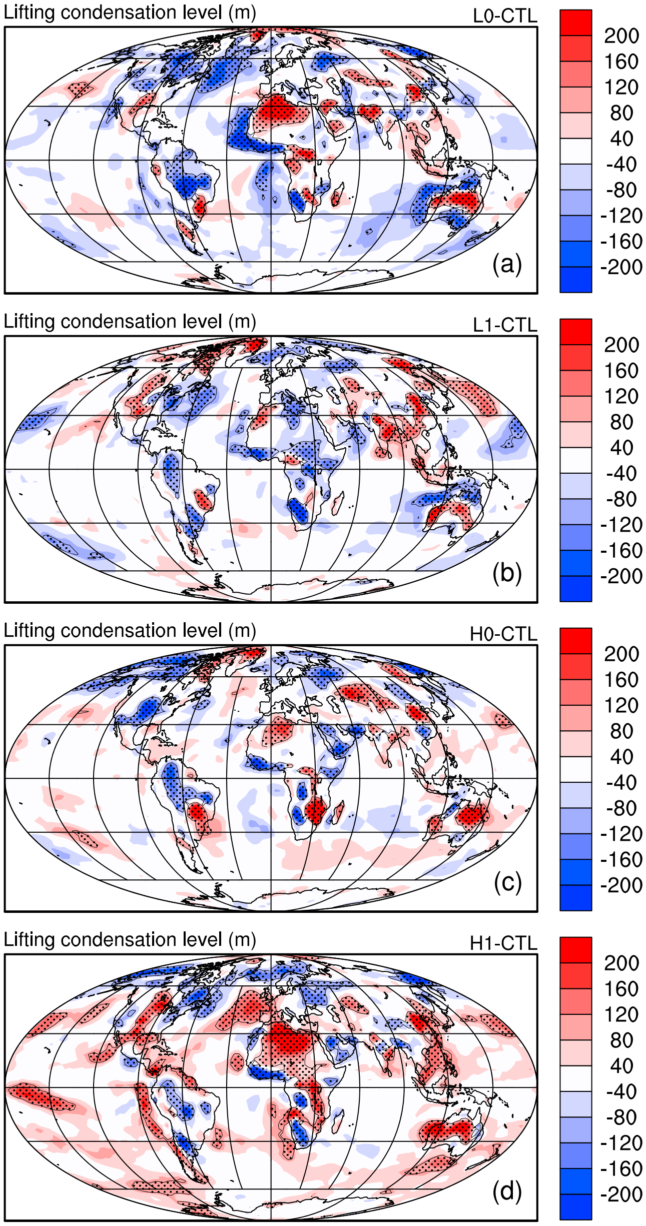

Figure 16. Same as Figure 4 but for lifting condensation level.

over the significant grid cells is $-0.25\,\mathrm{m\,s^{-1}}$ at the 0.993 sigma level, and the largest decrease is $-0.46\,\mathrm{m\,s^{-1}}$ at the 0.510 sigma level. This suggests that the Westerly Belt in the Southern Hemisphere may move south when a larger Ri_{cr} value is used. Changes in the west wind in the Northern Hemisphere are more complex because of the land-sea contrast.

The H1 experiment shows a slight increase of convective precipitation over the ocean surface around 60°S and a weak decrease of convective precipitation over the ocean surface around 45°S, but changes in stratiform precipitation, cloud fraction, and lifting condensation level are weak and insignificant.

4. Summary

The sensitivity of the BCC_AGCM climate model to the critical bulk Richardson number (Ri_{cr}) in the PBL parameterization has been investigated through a set of numerical experiments. Model output are intercompared for different values of Ri_{cr}. The main results are summarized below.

1. The globally averaged PBL height increases almost linearly with increasing Ri_{cr}. The global-averaged PBL height changes by about 114 m with a change of 0.5 in Ri_{cr}. Most prominent and significant changes in the PBL height occur in the Westerly Belt of the Southern Hemisphere. The globally averaged sensible (latent) heat flux decreases (increases) with increasing Ri_{cr}. The most significant changes in sensible heat flux occur over the middle-high-latitude ocean in the Southern Hemisphere, while the most significant changes in latent heat flux occur over arid continent areas in the Northern Hemisphere.
2. The impacts of increasing Ri_{cr} on globally averaged temperature, specific humidity, and wind speed are weak, and changes in temperature and specific humidity in the sensitivity experiments did not pass the significant test. Over the ocean in the Southern hemisphere, the west-east wind component strengthened around 60°S and weakened around 30°S as the Ri_{cr} increases, suggesting that the Westerly Belt may move south when a larger Ri_{cr} value is used.
3. Both convective precipitation and stratiform precipitation change with Ri_{cr}, but the changes are different for convective precipitation and stratiform precipitation. Globally averaged stratiform precipitation increases with increasing Ri_{cr}, whereas increasing Ri_{cr} mainly redistributes the convective precipitation. Strong and significant changes in convective precipitation occur over the ITCZ, while changes in

stratiform precipitation are more significant over arid land areas where significant changes in latent heat flux are also observed. The influence of changing Ri_{cr} on the lifting condensation level is nonlinear and complicated.

4. Although the globally averaged impacts of Ri_{cr} value on PBL height, surface fluxes, and other meteorological fields are not dramatic, the spatial distributions of these impacts are inhomogeneous. Thus, the impacts on regional and local climates can be important. This paper is a first step of our analyses focusing on the global picture. Higher-resolution simulations and detailed comparisons to observations are needed in future investigations.

Acknowledgments
This paper is supported by the National Basic Research Program of China (2011CB952002), China Meteorological Administration (GYHY201006024), and the National Natural Science Foundation of China (41375014). Yangang Liu is supported by the U.S. Department of Energy's Earth Modeling Program (ESM) via the FASTER project (www.bnl.gov/faster) and Atmospheric System Research program. .The authors are particularly grateful to three anonymous reviewers for their careful review and valuable comments, which led to substantial improvement of this manuscript. The data and code (in FORTRAN language) used in this paper can be obtained from the first author.

References

Basu, S., A. A. M. Holtslag, L. Caporaso, A. Riccio, and G. J. Steeneveld (2014), Observational support for the stability dependence of the bulk Richardson number across the stable boundary layer, *Boundary Layer Meteorol.*, *150*, 515–523.

Bretherton, C. S., and S. Park (2009), A new moist turbulence parameterization in the community atmosphere model, *J. Clim.*, *22*, 3422–3448.

Findell, K., and F. Eltahir (2003), Atmospheric controls on soil moisture–boundary layer interactions. Part I: Framework development, *J. Hydrometeorol.*, *4*(3), 552–569.

Grachev, A. A., E. L. Andreas, C. W. Fairall, P. S. Guest, and P. O. G. Persson (2013), The critical Richardson number and limits of applicability of local similarity theory in the stable boundary layer, *Boundary Layer Meteorol.*, *147*, 51–82.

Holtslag, A. A. M., and B. A. Boville (1993), Local versus nonlocal boundary layer diffusion in a global climate model, *J. Clim.*, *6*(10), 1825–1842.

Katul, G. G., A. Porporato, S. Shah, and E. Bou-Zeid (2014), Two phenomenological constants explain similarity laws in stably stratified turbulence, *Phys. Rev. E: Stat. Nonlinear Soft Matter Phys.*, *89*, doi:10.1103/PhysRevE.89.023007.

Kiehl, J. T., J. J. Hack, G. B. Bonan, B. A. Boville, D. L. Williamson, and P. J. Rasch (1998), The National Center for Atmospheric Research Community Climate Model: CCM3, *J. Clim.*, *11*(6), 1131–1149.

Liu, G., Y. Liu, and S. Endo (2013), Evaluation of surface flux parameterizations with long-term ARM observations, *Mon. Weather Rev.*, *141*, 773–797.

Louis, J. F. (1979), A parametric model of vertical eddy fluxes in the atmosphere, *Boundary Layer Meteorol.*, *17*(2), 187–202.

Miles, J. W. (1961), On the stability of heterogeneous shear flows, *J. Fluid Mech.*, *10*, 496–508.

Noh, Y., W. G. Cheon, S. Y. Hong, and S. Raasch (2003), Improvement of the K-profile model for the planetary boundary layer based on large eddy simulation data, *Boundary Layer Meteorol.*, *107*(2), 401–427.

Park, S., and C. S. Bretherton (2009), The University of Washington shallow convection and moist turbulence schemes and their impact on climate simulations with the Community Atmosphere Model, *J. Clim.*, *22*, 3449–3469.

Richardson, H., S. Basu, and A. A. M. Holtslag (2013), Improving stable boundary-layer height estimation using a stability-dependent critical bulk Richardson number, *Boundary Layer Meteorol.*, *148*, 93–109.

Shin, S.-H., and K.-J. Ha (2007), Effects of spatial and temporal variations in PBL depth on a GCM, *J. Clim.*, *20*, 4717–4732.

Stull, R. B. (1988), An introduction to boundary layer meteorology, Kluwer Acad., Norwell, Mass.

Troen, I., and L. Mahrt (1986), A simple model of the atmospheric boundary layer: Sensitivity to surface evaporation, *Boundary Layer Meteorol.*, *37*(1–2), 129–148.

Vogelezang, D. H. P., and A. A. M. Holtslag (1996), Evaluation and model impacts of alternative boundary-layer height formulations, *Boundary layer Meteorol.*, *81*, 245–269.

Wu, T., R. Yu, and F. Zhang (2008), A modified dynamic framework for atmospheric spectral model and its application, *J. Atmos. Sci.*, *65*, 2235–2253.

Wu, T., R. Yu, F. Zhang, Z. Wang, M. Dong, L. Wang, X. Jin, D. Chen, and L. Li (2010), The Beijing Climate Center atmospheric general circulation model: Description and its performance for the present-day climate, *Clim. Dyn.*, *34*, 123–147.

Yamada, T. (1975), The critical Richardson number and the ratio of the eddy transport coefficients obtained from a turbulence closure model, *J. Atmos. Sci.*, *32*, 926–933.

Yao, M.-S., and Y. Cheng (2012), Cloud simulations in response to turbulence parameterizations in the GISS Model E GCM, *J. Clim.*, *25*, 4963–4974.

Zhang, G., and N. A. McFarlane (1995), Sensitivity of climate simulations to the parameterization of cumulus convection in the Canadian Climate Centre general circulation model, *Atmos. Ocean*, *33*, 407–446.

Zhang, G., and M. Mu (2005), Effects of modifications to the Zhang-McFarlane convection parameterization on the simulation of the tropical precipitation in the National Center for Atmospheric Research Community Climate Model, version 3, *J. Geophys. Res.*, *110*, D09109, doi:10.1029/2004JD005617.

Zhang, Y., Z. Gao, D. Li, Y. Li, N. Zhang, X. Zhao, and J. Chen (2014), On the computation of planetary boundary layer height using the bulk Richardson number method, *Geosci. Model Dev.*, *7*, 2599–2611.